AIAA JOURNAL
Vol. 34, No. 11, November 1996

# Layerwise Mechanics and Finite Element Model for Laminated Piezoelectric Shells

Paul Heyliger* and K. C. Pei†
*Colorado State University, Fort Collins, Colorado 80523*
and
Dimitris Saravanos‡
*Ohio Aerospace Institute, Cleveland, Ohio 44142*

**A discrete-layer shell theory and associated finite element model is constructed for general laminated piezoelectric composite shells. The discrete-layer shell theory is based on linear piezoelectricity and accounts for general through-thickness variations of displacement and electrostatic potential by implementing one-dimensional piecewise continuous Lagrange interpolation approximations over a specified number of sublayers. The formulation applies to shells of general shape and lamination. Initially, the static and dynamic behavior of a simply supported flat plate is studied to compare with available exact solutions, with excellent agreement being obtained. Static loading and free vibration of a cylindrical ring are then considered to evaluate the element and to study the fundamental behavior of active/sensory piezoelectric shells.**

## Introduction

THE mechanical and electrical behavior of general curvilinear shells with embedded or surface piezoelectric layers is seeing renewed interest in the field of adaptive structures. As more demanding applications are investigated for this class of structure, a more accurate representation of the coupled fields is required over more simplified models developed in the past. As with other coupled-field mechanics problems, exact or analytical solutions are possible for only a very few select geometries. Approximate methods, such as finite elements, provide an accurate and powerful alternative for studying such solids.

The basic theory of linear piezoelectricity has been outlined by several authors.[1-4] Early computational studies of piezoelectric solids include those of Eer Nisse[5,6] and Holland[7] for electroelastic vibration analysis using the Ritz method. Allik and Hughes[8] introduced a finite element formulation for the equations of piezoelectricity. Other early finite element models of linear piezoelectricity were those of Kagawa and Yamabuchi,[9] Naillon and co-workers,[10] Ostergaard and Pawlak,[11] and Kunkel and co-workers.[12]

A number of approaches have been introduced to model laminated piezoelectric shells containing piezoelectric layers. Tzou and co-workers have presented a number of approaches for piezoelectric shells,[13-16] many of which used the Kirchoff–Love hypotheses for thin shells. Tzou also has presented a comprehensive treatment of the fundamental theory of piezoelectric shells.[17] Lammering[18] developed a shear-deformation finite element to analyze a shell structure with surface-coated piezoelectric layers. Dökmeci[19,20] also has studied the theoretical background of piezoelectric shell vibration.

Most theories developed for the analysis of laminated piezoelectric composites include limitations that may not represent the true behavior for certain applications. For the analysis of thick laminates, the Kirchoff–Love hypothesis for plate and shell geometries often yields poor approximations of interlaminar and intralaminar stress components.[21] In addition to this limitation, other previous studies have made use of an equivalent force representation of induced strain actuation in the piezoelectric laminate.[22] This kind of approach does not solve the coupled equations of piezoelectricity but attempts to mimic the piezoelectric effect indirectly. In most previously developed piezoelectric shell theories, assumptions have been made on the nature of the displacement and potential through the thickness of the laminate. This type of approach can provide reasonable results for thin shells, but such approximations diverge from reality when the shell becomes thick.

There is a need for novel piezoelectric shell theories and finite element approximations with robust capabilities in terms of modeling layer thicknesses, lamination, actuator and sensor response, and global and local response. To analyze thick laminated piezoelectric shells, cylindrical or general, the limitations described above require considerable refinement. In the present study, discrete-layer approximations are used through the plate thickness for the displacement and electrostatic potential components. The discrete-layer label refers to the thickness of the laminate being divided into a specific number of layers or elements and using standard finite element approximations through the thickness to model the behavior of the field. The nature of these approximations is such that those for the potential and the displacements can be identical to or different from each other.

Pauley[23] was among the first to use what can be described as a discrete-layer theory for piezoelectric solids in the analysis of free vibration characteristics of infinite laminated piezoelectric plates. Reddy[24] and Robbins and Reddy[25] have generalized this type of theory for elastic plates, and the corresponding coupled-field theory for piezoelectric plates has also been developed.[26,27] A discrete-layer finite element has been developed for laminated piezoelectric beams and plates,[28,29] which yielded good agreement with exact solutions.

In this study, a discrete-layer laminate model is presented for the analysis of laminated piezoelectric composite shells. The variational formulation and corresponding finite element model are developed using the equations of motion and the charge equation. For verification, the predicted static response and free vibration behavior for the flat plate are compared with exact solutions. The active/sensory and free vibration response of a piezoelectric/elastic ring is also studied.

## Governing Equations

### Linear Piezoelectricity

The equations of motion for a piezoelectric solid are given by

$$\tau_{ij,j} = \rho \ddot{u}_i \qquad i, j = 1, \ldots, 3 \tag{1}$$

Here $\tau_{ij}$ are the components of stress, $\rho$ is the material density, an overdot denotes differentiation with respect to time, and $u_i$ are the components of displacement. The charge equation of electrostatics is given in terms of the components of electric displacement $D_i$ as

$$D_{i,i} = 0 \qquad i = 1, \ldots, 3 \tag{2}$$

Received Aug. 31, 1995; revision received May 8, 1996; accepted for publication May 30, 1996; also published in *AIAA Journal in Disc*, Volume 1, Number 4. 

*Associate Professor, Department of Civil Engineering.
†Research Associate, Department of Civil Engineering.
‡Senior Research Associate, 22800 Cedar Point Road. Member AIAA.

The piezoelectric constitutive equations are given by

$$\tau_i = C_{ij} S_j - e_{ki} E_k \tag{3}$$

$$D_k = e_{kj} S_j + \varepsilon_{kl} E_l \qquad i, j = 1, \ldots, 6 \quad \text{and} \quad l, k = 1, \ldots, 3 \tag{4}$$

The elements $C_{ij}$ are the elastic stiffnesses, $e_{ki}$ are the piezoelectric coefficients, and $\varepsilon_{kl}$ are the dielectric constants. The components $S_j$ are the engineering strains, and the electric field components $E_k$ are related to the electrostatic potential $\phi$ by the relations

$$E_k = -\phi_{,k} \qquad k = 1, \ldots, 3 \tag{5}$$

The constitutive relations of an off-axis, orthotropic layer are assumed in this study.

**Variational Formulation**

*Global Cartesian System*

The weak form of the equations of motion for the shell can be written using Hamilton's principle for a linear piezoelectric medium in Cartesian coordinates. This forms the basis of the shell element presented in the sequel. This is given as[3]

$$\delta \int_{t_0}^{t_1} \mathrm{d}t \int_V \left[ \frac{1}{2} \rho \dot{u}_i \dot{u}_i - H(S_{kl}, E_k) \right] \mathrm{d}V + \int_{t_0}^{t_1} \mathrm{d}t \int_S (\hat{t}_i \delta u_i - \hat{\sigma} \delta \phi) \, \mathrm{d}S = 0 \tag{6}$$

Here, $t_0$ and $t_1$ are two arbitrary times, $\delta$ is the variational operator, $V$ and $S$ are the volume and surface of the solid, $\hat{t}_i$ and $\hat{\sigma}$ represent specified traction and surface charges, and $H$ is the electric enthalpy per unit volume. This latter term can be expressed in terms of the strain and electric-field components as

$$H(S_i, E_k) = \tfrac{1}{2} C_{ij} S_i S_j - e_{ki} E_k S_i - \tfrac{1}{2} \varepsilon_{kl} E_k E_l \tag{7}$$

*Local Curvilinear System*

The curvilinear coordinate system, described by $\xi$-, $\eta$-, and $\zeta$-coordinate directions, is the local system for the general shell, with $\bar{u}$, $\bar{v}$, $\bar{w}$ representing the components of displacement along the $\xi$-, $\eta$-, $\zeta$-coordinate directions. The $\zeta$ direction is located along the normal direction (also the poling direction) of the layer surface, and the $\xi$ and $\eta$ directions are tangent to the layer surface. In the subsequent derivation, overbars are used to denote the field variables in the local system. Global variables in $(x, y, z)$ are listed without an overbar.

The governing equations in Cartesian coordinates were outlined in the preceding section. The strain components in the global coordinate system can be transformed into the local system using the relations

$$\{\bar{\epsilon}\}_{\xi\eta\zeta} = \begin{Bmatrix} \bar{\epsilon}_{\xi\xi} \\ \bar{\epsilon}_{\eta\eta} \\ \bar{\epsilon}_{\zeta\zeta} \\ \bar{\epsilon}_{\eta\zeta} \\ \bar{\epsilon}_{\xi\zeta} \\ \bar{\epsilon}_{\xi\eta} \end{Bmatrix} = [T] \begin{Bmatrix} \epsilon_{xx} \\ \epsilon_{yy} \\ \epsilon_{zz} \\ \epsilon_{yz} \\ \epsilon_{xz} \\ \epsilon_{xy} \end{Bmatrix} = \begin{bmatrix} t_{11}^2 & t_{12}^2 & t_{13}^2 & 2t_{12}t_{13} & 2t_{11}t_{13} & 2t_{11}t_{12} \\ t_{21}^2 & t_{22}^2 & t_{23}^2 & 2t_{22}t_{23} & 2t_{21}t_{23} & 2t_{21}t_{22} \\ t_{31}^2 & t_{32}^2 & t_{33}^2 & 2t_{32}t_{33} & 2t_{31}t_{33} & 2t_{31}t_{32} \\ t_{21}t_{31} & t_{22}t_{32} & t_{23}t_{33} & t_{22}t_{33} + t_{23}t_{32} & t_{21}t_{33} + t_{23}t_{31} & t_{21}t_{32} + t_{22}t_{31} \\ t_{11}t_{31} & t_{12}t_{32} & t_{13}t_{33} & t_{12}t_{33} + t_{13}t_{32} & t_{11}t_{33} + t_{13}t_{31} & t_{11}t_{32} + t_{12}t_{31} \\ t_{11}t_{21} & t_{12}t_{22} & t_{13}t_{23} & t_{12}t_{23} + t_{13}t_{22} & t_{11}t_{23} + t_{13}t_{21} & t_{11}t_{22} + t_{12}t_{21} \end{bmatrix} \begin{Bmatrix} \epsilon_{xx} \\ \epsilon_{yy} \\ \epsilon_{zz} \\ \epsilon_{yz} \\ \epsilon_{xz} \\ \epsilon_{xy} \end{Bmatrix} \tag{8}$$

Here the elements $t_{ij}$ are scaled components of the transpose of the Jacobian matrix, expressed as

$$[t] = \begin{bmatrix} t_{11} & t_{12} & t_{13} \\ t_{21} & t_{22} & t_{23} \\ t_{31} & t_{32} & t_{33} \end{bmatrix} = \begin{bmatrix} \dfrac{\partial x}{h_\xi \partial \xi} & \dfrac{\partial y}{h_\xi \partial \xi} & \dfrac{\partial z}{h_\xi \partial \xi} \\ \dfrac{\partial x}{h_\eta \partial \eta} & \dfrac{\partial y}{h_\eta \partial \eta} & \dfrac{\partial z}{h_\eta \partial \eta} \\ \dfrac{\partial x}{h_\zeta \partial \zeta} & \dfrac{\partial y}{h_\zeta \partial \zeta} & \dfrac{\partial z}{h_\zeta \partial \zeta} \end{bmatrix} \tag{9}$$

The values $h_\xi$, $h_\eta$, and $h_\zeta$ are scaling factors denoting the ratio of the differential distances to the differentials of the coordinate parameters as commonly used in curvilinear coordinates.[30] For example, in the case of the circular cylindrical shell, the scaling factors are $h_\xi = h_z = 1$, $h_\eta = h_\theta = r$, and $h_\zeta = h_r = 1$.

The displacement and electric-field components in the two systems are related by

$$\begin{Bmatrix} \bar{u} \\ \bar{v} \\ \bar{w} \end{Bmatrix} = \left[ J\left( \frac{x, y, z}{\xi, \eta, \zeta} \right) \right]^T \begin{Bmatrix} u \\ v \\ w \end{Bmatrix} \tag{10}$$

$$\begin{Bmatrix} \bar{E}_\xi \\ \bar{E}_\eta \\ \bar{E}_\zeta \end{Bmatrix} = [t] \begin{Bmatrix} E_x \\ E_y \\ E_z \end{Bmatrix} \tag{11}$$

Here $[J]$ is the Jacobian matrix, taken as

$$\left[ J\left( \frac{x, y, z}{\xi, \eta, \zeta} \right) \right] = \begin{bmatrix} \dfrac{\partial x}{\partial \xi} & \dfrac{\partial x}{\partial \eta} & \dfrac{\partial x}{\partial \zeta} \\ \dfrac{\partial y}{\partial \xi} & \dfrac{\partial y}{\partial \eta} & \dfrac{\partial y}{\partial \zeta} \\ \dfrac{\partial z}{\partial \xi} & \dfrac{\partial z}{\partial \eta} & \dfrac{\partial z}{\partial \zeta} \end{bmatrix} = \begin{bmatrix} J_{11} & J_{12} & J_{13} \\ J_{21} & J_{22} & J_{23} \\ J_{31} & J_{32} & J_{33} \end{bmatrix} \tag{12}$$

Substitution of the constitutive equations yields the elastic stiffness matrix, the matrix of piezoelectric coefficients, and the dielectric constants in the curvilinear coordinate system. Then the variation of electric enthalpy in Eq. (7), $\delta H$, can be expressed as

$$\begin{aligned} \delta H &= \delta \lfloor \bar{S}_j, \bar{E}_i \rfloor_{\xi\eta\zeta} [R][C]_{\xi\eta\zeta} [R] \{\bar{S}_j, \bar{E}_i\}_{\xi\eta\zeta} \\ &= \delta \lfloor S_m, E_l \rfloor_{xyz} [R][C]_{xyz} [R] \{S_m, E_l\}_{xyz} \\ &= \delta \lfloor u_{l,m}, -\phi_{,l} \rfloor_{xyz} [B][C]_{xyz} [B]^T \{u_{l,m}, -\phi_{,l}\}_{xyz} \\ &= \delta \lfloor u_{i,j}, -\phi_{,i} \rfloor_{\xi\eta\zeta} [\bar{J}^*][B][C]_{xyz} [B]^T [\bar{J}^*]^T \{u_{i,j}, -\phi_{,i}\}_{\xi\eta\zeta} \end{aligned} \tag{13}$$

Here the vectors $\{\bar{S}_j, \bar{E}_i\}$ contain the components of strain and electric field, $[R]$ is a diagonal matrix containing the elements 1 or 2, the elements of $[C]$ represent the material properties, $[B]$ contains only the elements 1 or 0, and $[\bar{J}^*]$ contains $3 \times 3$ submatrices of the inverse of the Jacobian matrix. The explicit entries are listed elsewhere.[31]

The variational formulation in curvilinear coordinates can be derived using the above relationships and Eq. (6) as

$$\int_{t_0}^{t_1} \left\{ -\int_S (\delta \lfloor u, -\phi \rfloor_{\xi\eta\zeta} \{T\}_{\xi\eta\zeta}) \, \mathrm{d}S + \int_V (\delta \lfloor u, -\phi \rfloor_{\xi\eta\zeta} \times [\Upsilon] \{\ddot{u}, -\ddot{\phi}\}_{\xi\eta\zeta} + \delta \lfloor u_{i,j}, -\phi_{,j} \rfloor_{\xi\eta\zeta} [D] \{u_{i,j}, -\phi_{,j}\}_{\xi\eta\zeta}) \times \left| J\left( \frac{x, y, z}{\xi, \eta, \zeta} \right) \right| \mathrm{d}V_{\xi\eta\zeta} \right\} \mathrm{d}t = 0 \tag{14}$$

Here the following matrices have been introduced:

$$[D] = [\bar{J}^*][B][C]_{xyz}[B]^T[\bar{J}^*]^T \tag{15}$$

$$\delta\lfloor u, -\phi\rfloor_{\xi\eta\zeta} = \lfloor \delta u \quad \delta v \quad \delta w \quad -\delta\phi \rfloor \tag{16}$$

$$\lfloor \ddot{u} - \ddot{\phi}\rfloor_{\xi\eta\zeta} = \lfloor \ddot{u} \quad \ddot{v} \quad \ddot{w} \quad -\ddot{\phi}\rfloor \tag{17}$$

$$\{T\}_{\xi\eta\zeta} = \begin{Bmatrix} \hat{t}_\xi(\xi,\eta,\zeta) \\ \hat{t}_\eta(\xi,\eta,\zeta) \\ \hat{t}_\zeta(\xi,\eta,\zeta) \\ \hat{\sigma} \end{Bmatrix} \tag{18}$$

The matrix $[\Upsilon]$ is a $4 \times 4$ diagonal matrix with all nonzero entries equal to $\rho$ except $\Upsilon_{44}$, which is zero.

Equation (14) provides the basis of numerical (i.e., finite element) approximations and can also yield, with additional operations, the equations of motion and the charge equation. Only approximate solutions to the weak form are sought here. Critical in this step is the form of the through-thickness approximations for the displacement field and the electrostatic potential. This is described in the next section.

### Discrete-Layer Approach

In the kinematic/potential assumptions of the laminate shell theory developed in this study, independent piecewise approximations are used for the three displacement components and the electrostatic potential through the thickness of the shell in the local curvilinear coordinate system. Hence

$$\bar{u}(\xi,\eta,\zeta,t) = \sum_{a=1}^{p}\sum_{j=1}^{q} U_{ja}(t)\Psi_a^u(\xi,\eta)\psi_j^u(\zeta) \tag{19}$$

$$\bar{v}(\xi,\eta,\zeta,t) = \sum_{a=1}^{p}\sum_{j=1}^{q} V_{ja}(t)\Psi_a^v(\xi,\eta)\psi_j^v(\zeta) \tag{20}$$

$$\bar{w}(\xi,\eta,\zeta,t) = \sum_{a=1}^{p}\sum_{j=1}^{q} W_{ja}(t)\Psi_a^w(\xi,\eta)\psi_j^w(\zeta) \tag{21}$$

$$\bar{\phi}(\xi,\eta,\zeta,t) = \sum_{a=1}^{p}\sum_{j=1}^{q} \Phi_{ja}(t)\Psi_a^\phi(\xi,\eta)\psi_j^\phi(\zeta) \tag{22}$$

where $p$ and $q$ are the number of terms in the surface and thickness approximations, respectively.

Two levels of approximation are implicit in this step: one in the surface of the shell as denoted by the functions $\Psi(\xi,\eta)$ and the other through the thickness as denoted by the functions $\psi(\zeta)$. This allows the thickness behavior to be preintegrated in a manner similar to most other plate and shell theories, with the in-surface approximation then taking a form similar to standard finite element models.

Using these conditions for the displacements and electrostatic potential, theories may be developed for a wide range of behaviors. For example, a theory with a constant transverse displacement can be developed that reduces the number of degrees of freedom and results in a simpler model and more economical computation. However, poor accuracy can result by neglecting the through-thickness actuation strain, using this form of approximation. Allowing the transverse strain to be nonzero is a more complex and computationally demanding algorithm, but results in improved accuracy. In general, independent approximations of the displacements and potential allow a number of different types of behavior using the same theory. The formulation of the element matrices in this study reflects these independent approximations.

### Finite Element Approximation

The weak form of the governing equation using curvilinear coordinates was shown in the previous section and is used to allow for easier integration of the element matrices for a shell with arbitrary geometry. For each of the Gauss points, the numerical integration can be accomplished by mapping the discrete-layer shell element into a parent element in the local curvilinear coordinate space. In this manner, local element matrices are generated that are similar to those of the discrete-layer plate element.[28] These matrices can be transformed to the global system using the integral transformation rule

$$\int_{V_e} \mathrm{d}x\,\mathrm{d}y\,\mathrm{d}z = \int_{\bar{V}_e} |J|\,\mathrm{d}\xi\,\mathrm{d}\eta\,\mathrm{d}\zeta \tag{23}$$

where $\bar{V}_e$ is the volume of the parent element. Quadratic in-surface approximations $\Psi_a$ are used in the calculations to allow representation of the curved edges. This order of approximation can be modified easily for more simple or more complex geometries.

The geometry of the laminated shell element can be described in standard fashion as[32]

$$\begin{Bmatrix} x \\ y \\ z \end{Bmatrix} = \sum_{i=1}^{n} N_i(\xi,\eta,\zeta) \begin{Bmatrix} x_i \\ y_i \\ z_i \end{Bmatrix} \tag{24}$$

Here $(x, y, z)$ represents the location of a generic point within the shell element, $(x_i, y_i, z_i)$ are the locations of element nodes, and $n$ is the number of nodes in the element. The function $N_i$ indicates the shape function corresponding to the node $i$. If the curvilinear coordinate systems used in each layer are the same, the geometry of this element can be defined using only the locations of the nodal points on any two layer surfaces. These are usually taken as the top and bottom surfaces of the element. If multiple curvilinear coordinate systems are required, additional locations are required.

Substituting these approximations into the weak form of Eq. (14) allows the governing equations of the discretized system to be written in matrix form as

$$\begin{bmatrix} [M^{11}] & [0] & [0] & [0] \\ [0] & [M^{22}] & [0] & [0] \\ [0] & [0] & [M^{33}] & [0] \\ [0] & [0] & [0] & [0] \end{bmatrix} \begin{Bmatrix} \{\ddot{U}\} \\ \{\ddot{V}\} \\ \{\ddot{W}\} \\ \{\ddot{\Phi}\} \end{Bmatrix} + \begin{bmatrix} [K^{11}] & [K^{12}] & [K^{13}] & [K^{14}] \\ [K^{21}] & [K^{22}] & [K^{23}] & [K^{24}] \\ [K^{31}] & [K^{32}] & [K^{33}] & [K^{34}] \\ [K^{41}] & [K^{42}] & [K^{43}] & [K^{44}] \end{bmatrix} \begin{Bmatrix} \{U\} \\ \{V\} \\ \{W\} \\ \{\Phi\} \end{Bmatrix} = \begin{Bmatrix} \{F^1\} \\ \{F^2\} \\ \{F^3\} \\ \{Q\} \end{Bmatrix} \tag{25}$$

The elements of these equations are listed elsewhere[31] and are functions of both the preintegrated through-thickness approximation functions and those in the surface of the shell. This form of the equations of motion is similar to those of the piezoelectric beam and plate structures, and the solution procedure is described in detail elsewhere.[29]

## Numerical Examples

In this section, the shell element is applied to model the response of plate and shell composite laminates with distributed piezoelectric actuators/sensors. The results provide a test of the accuracy of the formulation, and an opportunity to understand how these laminates behave. Initial comparisons and convergence studies are made with an exact solution for simly supported piezoelectric plates.[33] Attention then is turned to a cylindrical titanium ring with an attached continuous piezoelectric layer. The properties for all materials described in this section are given in Table 1. The properties for the lead zirconate titanate (PZT) are from Berlincourt and co-workers,[34] and those of the polyvinylidene fluoride (PVDF) are from Tashiro and co-workers.[35] The properties for the nonpiezoelectric material are typical of a titanium alloy.

The level of approximation used in these examples is focussed on both the through-thickness or discrete-layer approximation and the in-plane approximation. For these examples, it is assumed that the through-thickness approximation functions used in Eqs. (19–22) are such that $\psi_j^u(\zeta) = \psi_j^v(\zeta) = \psi_j^w(\zeta) = \psi_j^\phi(\zeta)$, where these functions are taken to be linear Lagrangian interpolation polynomials. The simplified model corresponding to these fields implies a piecewise linear behavior of the electroelastic fields through the thickness of the laminate for all unknown quantities. The grading can be as fine

as possible by using more layers to describe the thickness dimension. Quadratic approximations are used in the surface of the shell. One objective of this section is to assess the necessary number of elements in both thickness and tangential directions to achieve acceptable results. For the plate examples, a $3 \times 3$ Gaussian integration rule was used in-plane, with a single point used through the thickness. For the general shell problems, a $10 \times 10$ rule was used in the surface, with five points used through the thickness.

**Simply Supported Plates**

The static and free vibration behavior of a simply supported, square, laminated piezoelectric plate are studied. Specifically, results with various element configurations in the plane and discrete-layers through thickness are compared with the exact solutions to assess the convergence properties of the element and also to ensure the accuracy of the formulation and computational algorithm.

The simple-support conditions require that the normal stress, transverse displacement, tangential displacement, and electrostatic potential be zero around the plate edges. The top and bottom surfaces were assumed to be stress free.

**Table 1 Material properties**

| Property | Material PZT-5A | PZT-4 | PVDF | Passive |
|---|---|---|---|---|
| | *Elastic moduli, GPa* | | | |
| $E_1$ | 61.0 | 81.3 | 237.0 | 114.0 |
| $E_2$ | 61.0 | 81.3 | 23.2 | 114.0 |
| $E_3$ | 53.2 | 64.5 | 10.5 | 114.0 |
| | *Shear moduli, GPa* | | | |
| $G_{23}$ | 21.1 | 25.6 | 2.15 | 43.846 |
| $G_{13}$ | 21.1 | 25.6 | 4.40 | 43.846 |
| $G_{12}$ | 22.593 | 30.587 | 6.43 | 43.846 |
| | *Poisson ratios* | | | |
| $\nu_{12}$ | 0.350 | 0.329 | 0.154 | 0.3 |
| $\nu_{13}$ | 0.440 | 0.432 | 0.178 | 0.3 |
| $\nu_{21}$ | 0.350 | 0.329 | 0.015 | 0.3 |
| $\nu_{23}$ | 0.440 | 0.432 | 0.177 | 0.3 |
| $\nu_{31}$ | 0.384 | 0.343 | 0.008 | 0.3 |
| $\nu_{32}$ | 0.384 | 0.343 | 0.080 | 0.3 |
| | *Density, kg/m*$^3$ | | | |
| $\rho$ | 7700 | 7600 | —— | 2768 |
| | *Piezoelectric constants, C/m*$^2$ | | | |
| $e_{31}$ | −5.35 | −5.20 | −0.13 | 0.0 |
| $e_{32}$ | −5.35 | −5.20 | −0.14 | 0.0 |
| $e_{33}$ | 15.78 | 15.08 | −0.28 | 0.0 |
| $e_{24}$ | 12.29 | 12.72 | −0.01 | 0.0 |
| $e_{15}$ | 12.29 | 12.72 | −0.01 | 0.0 |
| | *Permittivities* ($\epsilon_0 = 8.85 \times 10^{-12}$), $C^2/(Nm^2)$ | | | |
| $\epsilon_{11}/\epsilon_0$ | 1730.0 | 1475.0 | 1.0 | 1.0 |
| $\epsilon_{22}/\epsilon_0$ | 1730.0 | 1475.0 | 1.0 | 1.0 |
| $\epsilon_{33}/\epsilon_0$ | 1700.0 | 1300.0 | 11.98 | 1.0 |

*Active Static Response*

The laminate configuration studied for the static case is a four-layer cross ply $[0/90]_s$ of PVDF. The span/thickness ratio is 10, with the total plate thickness 0.2 m. From symmetry, a quarter of the plate was modeled. The applied potential along the top surface is given by

$$\phi(x, y) = \sin(\pi x/L_x)\sin(\pi y/L_y) \tag{26}$$

where $L_x$ and $L_y$ are the lengths of the plate in the $x$ and $y$ directions, respectively. The bottom of the plate is held at zero potential.

The convergence of the induced maximum in-plane and transverse displacements and the electric enthalpy are studied. The respective exact values for the displacement and potential are generated using the methodology developed in the work of Heyliger,[33] with the values taken from Heyliger and co-workers.[31] These are shown in Table 2. Two different types of refinement are explored. In the first, the number of discrete layers is held constant and the in-plane mesh density is varied. The resulting displacements at several locations are shown in Table 2a. In the second refinement, the in-plane mesh density is fixed ($4 \times 4$) and the number of discrete layers through the thickness is changed. These results are shown in Table 2b. It appears from these examples that increasing the number of layers yields more dramatic changes in the field values, with two layers per ply or eight total layers yielding displacements within differences less than 1% of the exact solution. Both cases illustrate the excellent convergence of the element.

*Free Vibration*

Exact solutions are also available for the free vibration analysis of simply supported cross-ply laminated piezoelectric plates.[36] The convergence of the natural frequencies are studied for a single-ply square plate composed of PZT-4 with thickness of 0.2 m. The thickness aspect ratio is fixed at 10. Both closed ($\phi = 0$) and open ($D_z = 0$) circuit conditions are considered for the upper and lower surfaces of the plate. Because symmetry was used to model the plate, only those modes symmetric about $x = L_x/2$ and $y = L_y/2$ are studied. The in-plane dependence of the transverse displacements in this case take the form

$$w(x, y) = w_0 \sin(m\pi x/L_x)\sin(n\pi y/L_y) \tag{27}$$

Because symmetry is used to study the plate vibration, $m$ and $n$ must be odd integers when comparing with the exact solution.

The results are shown in Table 3. As before, the number of discrete layers has a much more dramatic impact on the resulting frequencies. Modes 1, 2, and 6 are the first three thickness modes corresponding to the fundamental in-plane mode with $m = n = 1$ in Eq. (27). Modes 3

**Table 2 Convergence of cross-ply, simply supported plate under sinusoidal potential ($a/h = 10$)**

| Mesh density (eight layers) | Displacement: Max. $w$ on bottom, $10^{-8}$ m | Max. $w$ on top, $10^{-8}$ m | Max. $u$ $10^{-9}$ m | Max. $v$ $10^{-9}$ m | Enthalpy, $10^{-3}$ |
|---|---|---|---|---|---|
| | *a. In-plane convergence* ($n = 8$) | | | | |
| $1 \times 1$ | −0.11189583 | 0.14752036 | 0.20423266 | 0.27674482 | −0.64994256 |
| $2 \times 2$ | −0.11189772 | 0.14793297 | 0.20777336 | 0.28230876 | −0.70814223 |
| $3 \times 3$ | −0.11197956 | 0.14801142 | 0.20807069 | 0.28239703 | −0.71184901 |
| $4 \times 4$ | −0.11201025 | 0.14803477 | 0.20811595 | 0.28234158 | −0.71249253 |
| $5 \times 5$ | −0.11202296 | 0.14804334 | 0.20812764 | 0.28230966 | −0.71267038 |
| Exact | −0.11202681 | 0.14807190 | 0.20949313 | 0.28351883 | —— |
| No. of discrete layers, $n$ | Displacement: Max. $w$ on bottom, $10^{-8}$ m | Max. $w$ on top, $10^{-8}$ m | Max. $u$, $10^{-9}$ m | Max. $v$, $10^{-9}$ m | Enthalpy $10^{-3}$ |
| | *b. Through-thickness convergence* ($4 \times 4$ *mesh*) | | | | |
| 4 | −0.11203254 | 0.14798181 | 0.20401336 | 0.27859397 | −0.71247648 |
| 8 | −0.11201025 | 0.14803477 | 0.20811595 | 0.28234158 | −0.71249253 |
| 12 | −0.11200459 | 0.14804562 | 0.20889647 | 0.28305034 | −0.71249551 |
| 16 | −0.11200244 | 0.14804944 | 0.20917435 | 0.28330048 | −0.71249656 |
| Exact | −0.11202681 | 0.14807190 | 0.20949313 | 0.28351883 | —— |

**Table 3 Frequencies from group 3, $a/h$ = 10, closed condition**

| Mesh density | Frequency, Hz | | | | |
|---|---|---|---|---|---|
| | Mode 1 | Mode 2 | Modes 3 and 4 | Mode 5 | Mode 6 |
| Four layers ($x \times y - 4$) | | | | | |
| $4 \times 4 - 4$ | 2894.1092 | 12367.145 | 12914.600 | 21245.604 | 21278.430 |
| $5 \times 5 - 4$ | 2893.7028 | 12366.870 | 12877.589 | 21185.786 | 21278.272 |
| $6 \times 6 - 4$ | 2893.5530 | 12366.769 | 12863.805 | 21166.096 | 21278.214 |
| $n$ layers ($4 \times 4 - n$). | | | | | |
| $4 \times 4 - 4$ | 2894.1092 | 12367.145 | 12914.600 | 21245.604 | 21278.430 |
| $4 \times 4 - 6$ | 2879.3854 | 12367.145 | 12844.945 | 21126.952 | 21277.624 |
| $4 \times 4 - 8$ | 2874.1758 | 12367.144 | 12819.610 | 21082.978 | 21277.342 |
| $4 \times 4 - 10$ | 2871.7544 | 12367.144 | 12807.702 | 21062.168 | 21277.210 |
| Six layers | | | | | |
| $6 \times 6 - 6$ | 2878.8370 | 12366.769 | 12794.567 | 21047.674 | 21277.408 |
| Exact | 2866.9217 | 12366.673 | 12723.534 | 20929.08 | 21278.220 |

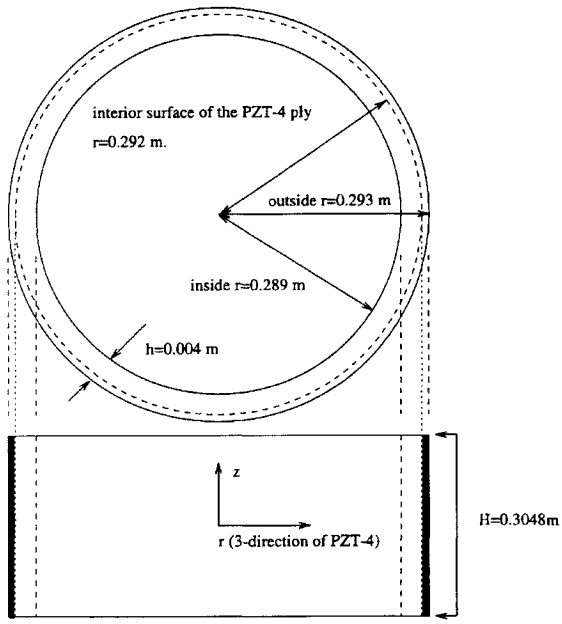


**Fig. 1 Domain and geometry of cylindrical ring.**

and 4 correspond to the in-plane modes with $m = 1, n = 3$, and $m = 3, n = 1$. Mode 5 is the first thickness mode corresponding to the in-plane mode $m = n = 3$. The higher in-plane modes are in poorer agreement with the exact solution because it is more difficult for the mesh to capture the higher in-plane behavior, whereas the higher thickness modes for $m = n = 1$ are well represented. Hence there is excellent convergence and agreement for the thickness modes for $m = n = 1$, with larger differences for the higher in-plane modes. This agreement indicates an accurate computational model.

### Cylindrical Ring

A circular cylindrical ring is studied next. The geometry of the cylinder is described in cylindrical coordinates $(r, \theta, z)$, as shown in Fig. 1. The dimensions of the ring are defined by the height $H = 0.3048$ m, the inner radius $r_i = 0.289$ m, and the total thickness $h$. The laminate has two layers. The passive inner layer is constructed of titanium and the outer layer is PZT-4. The two layers are assumed to be perfectly bonded. In some examples the total thickness of the laminate may vary, but the thickness ratio of the titanium to the PZT-4 is fixed at 3.

In all examples, symmetry is exploited to reduce the computational size of the problem. One-quarter of the shell is typically modeled. At times, it is also possible to reduce the quarter shell into two halves in the $z$ direction if symmetry permits. Hence the original ring is divided into eight equal-sized sections, and the analysis is completed on a single section. Appropriate boundary conditions on the displacements and potential are imposed to simulate the response of the complete ring. For instance, the case of quarter symmetry yields the physical quantities of homogeneous normal displacement, shear traction, and electric displacement along the lines of symmetry. In some cases, the results are presented for the modeled domain, but in all cases are representative of the complete shell. Different mesh representations were used for each example and are noted below.

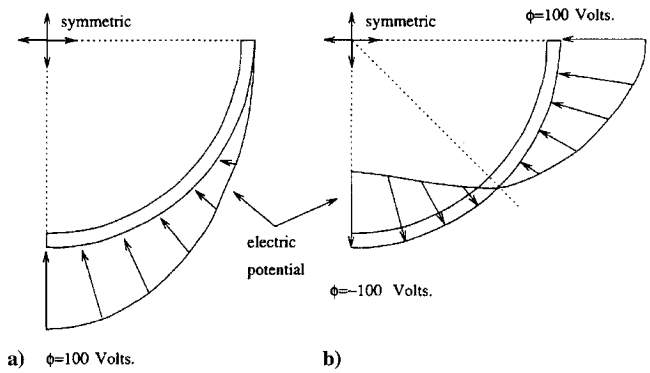


**Fig. 2 Applied surface potentials.**

*Active Static Behavior*

A surface potential is first applied to the thin ($t = 0.004$ m) shell at the outer surface defined by $r_o$. There are two electric potential fields applied: case a, with $\phi(\theta) = 100 \sin|\theta|$, and case b, with $\phi(\theta) = 100 \cos|2\theta|$. These are shown schematically in Figs. 2a and 2b, respectively. In each case, the potential at the inner surface of the active layer (i.e., the interface between the two materials) is fixed at zero. The thickness of the inner passive layer is 0.003 m, and that of the outer active layer 0.001 m. A mesh discretization of $20 \times 2 \times 8$ was used, with 20 elements in the circumferential direction, 2 in the axial half-direction using symmetry, and 8 discrete layers. The radial displacement at $r = 0.289$ m and $z = 0$ as a function of angle is shown in Figs. 3a and 3b for cases a and b, respectively.

Examination of the radial displacement shows that this quantity is much larger for the case of $\phi(\theta) = 100 \cos|2\theta|$ (case b) than for $\phi(\theta) = 100 \sin|\theta|$ (case a). This is so even though the maximum potential is the same in both cases. The applied potential distribution of case b matches the circumferential behavior of the natural mode of deformation for the radial displacement, which can be observed by considering the symmetric extension of the applied potentials in Fig. 2. In case a, the applied potential does not correspond to any fundamental deformation pattern because it is always positive or zero around the circumference of the ring. This provides a simple demonstration of the differences in actuation for this structure for a fixed maximum applied potential. Such a procedure can and has been extended by others to optimize actuation for a particular mode of deformation.

Representative normal and shear stress components are shown in Figs. 4a and 4b for the case of a thick ($h = 0.04$ m) two-ply shell with the applied potential of case b. The stresses are computed using the constitutive equations at the element centroids, with the exceptions of the normal radial stress and the transverse shear stress $\sigma_{r\theta}$ at the inner and outer surfaces. These values are set to zero from the traction-free condition at these locations.

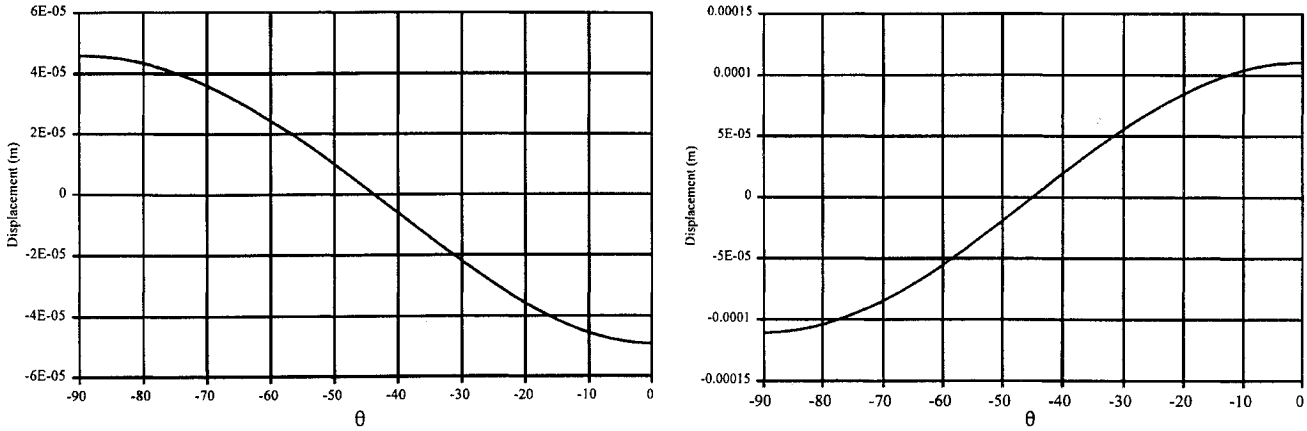


a) $\phi = 100 \sin|\theta|$ b) $\phi = 100 \cos 2|\theta|$

**Fig. 3 Radial displacement distributions for applied surface potentials in two-ply ring.**

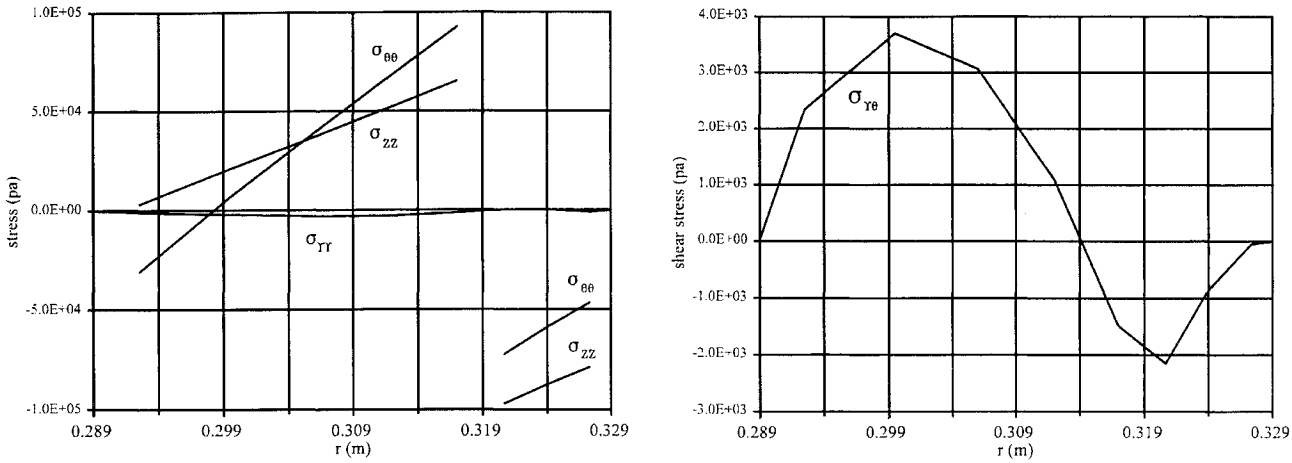


a) Normal stresses b) Transverse shear stress $\sigma_{r\theta}$

**Fig. 4 Stress distributions for thick two-ply shell.**

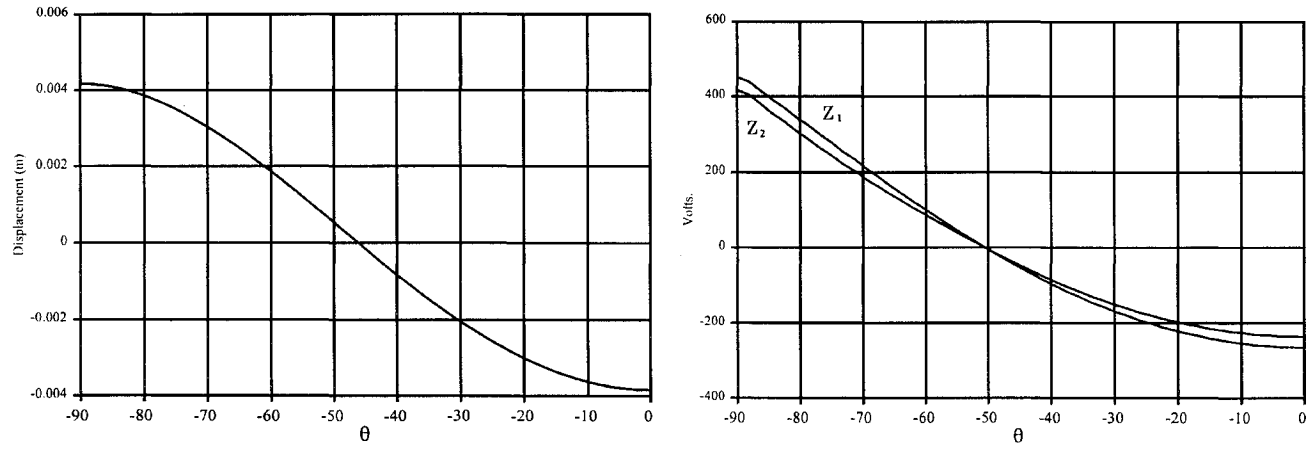


a) Radial displacement b) Electrostatic potential at $r = 0.291$ m

**Fig. 5 Distributions for thin single-ply of PZT-4 under line loading.**

The normal stresses are shown in Fig. 4a and are plotted through the thickness at $\theta = 0$ and $z = 0$. The normal stress $\sigma_{rr}$ tends to zero to satisfy the homogeneous normal traction condition at the outer and inner surfaces. The circumferential stress is slightly higher than the axial stress in the titanium layer, but this trend is reversed in the PZT layer. The plots do not continue to the outer and inner surfaces because stresses are computed at the layer centroids. There is a jump in the stresses across the dissimilar interface caused by the mismatch in material properties. The shear stress is shown in Fig. 4b and is plotted through the thickness at $\theta = 45$ deg and $z = 0$.

*Sensory Static Behavior*

A thin shell with $h = 0.004$ and a thicker shell with $h = 0.04$ m are considered under a line loading applied at $\pm 90$ deg, with the magnitude 656.17 N/m. This is equivalent to a load of 200 N per thickness of the $z$ dimension of the shell. The shell is a single layer of PZT-4. The mesh representation for this example is $24 \times 2 \times 4$ for the thin shell and $16 \times 2 \times 9$ for the thick shell. Both the inner and outer surfaces of the shell are fixed at zero potential. The resulting radial displacements and electrostatic potential at $r = 0.289$ m are shown in Figs. 5a and 5b for the thin shell and Figs. 6a and 6b for

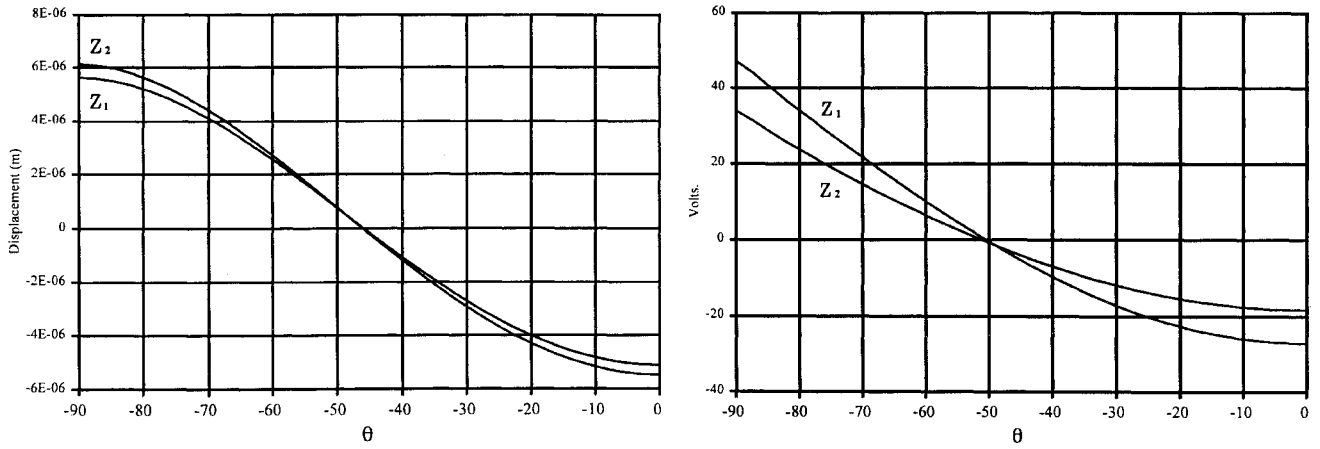


a) Radial displacement

b) Electrostatic potential at $r = 0.30678$ m

**Fig. 6 Distributions for thick single ply of PZT-4 under line loading.**

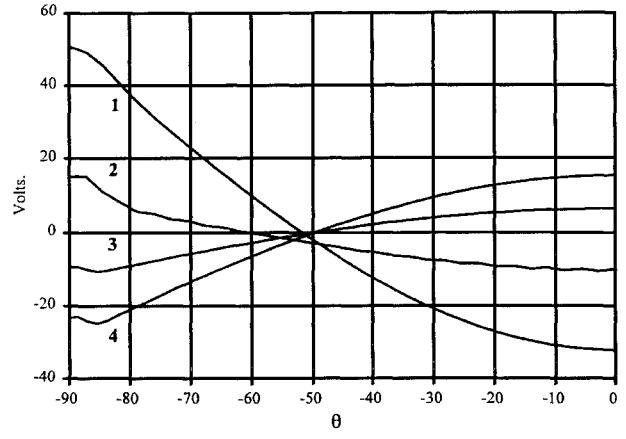


**Fig. 7 Potential distributions for thick shells under line load with no surface grounding.**

the thick shell. In these plots, the curves labeled $z_1$ represent the distributions at $z = 0$, and $z_2$ are those at $z = 0.1524$ m. There is a negligible difference in $z$ dependence on the radial displacement for the thin shell. For the thin shell potential and the displacement and potential in the thick shell, a solid line is used to denote the distribution at $z = 0$ and the crosses for that at $z = 0.1524$ m. The slight but noticeable dependence of the potential on $z$ is partially explained by the condition of zero axial traction on the end faces of the cylinder but nonzero axial stress at the axial midlength.

The loading condition is repeated for the thick single layer of PZT-4 and the thick two-layer shell. Both have total thickness of 0.04 m. The single layer is grounded on the interior surface as before. For the two-ply shell, the thickness of the active layer is 0.01m and the interface between the two is held at zero potential. The outer surface for both shells is no longer fixed at zero potential. The mesh for the single layer is $16 \times 2 \times 9$ and that for the two-layer shell is $28 \times 2 \times 5$. The resulting distributions of electrostatic potential on the surface and within the PZT-4 layer at $z = 0$ are shown in Fig. 7. Curves 1, 2, 3, and 4 represent the distributions for the PZT-4 shell at $r = 0.309$, the PZT-4 shell at $r = 0.329$, the two-ply shell at $r = 0.324$, and the two-ply shell at $r = 0.329$, respectively. The small disturbances near $\theta = -90$ are related to the application of the point load at these locations.

*Free Vibration Response*

The natural frequencies of free vibration were computed for the thin ($t = 0.004$ m) configuration of the single- and two-layer shells. Because there are three planes of symmetry for free vibration, eight different sets of displacement boundary conditions can be applied

**Table 4 Homogeneous displacement components occurring on the surfaces $x = 0, y = 0$, and $z = 0$ of the part of the cylindrical shells**

| Group no. | Boundary conditions | | | | | | | | |
|---|---|---|---|---|---|---|---|---|---|
| | $x = 0$ | | | $y = 0$ | | | $z = 0$ | | |
| | $u_r$ | $u_\theta$ | $u_z$ | $u_r$ | $u_\theta$ | $u_z$ | $u_r$ | $u_\theta$ | $u_z$ |
| 1 | 0 | — | 0 | 0 | — | 0 | 0 | 0 | |
| 2 | 0 | — | 0 | — | 0 | — | 0 | 0 | — |
| 3 | — | 0 | — | — | 0 | — | 0 | 0 | — |
| 4 | — | 0 | — | 0 | — | 0 | 0 | 0 | — |
| 5 | 0 | — | 0 | 0 | — | 0 | — | — | 0 |
| 6 | 0 | — | 0 | — | 0 | — | — | — | 0 |
| 7 | — | 0 | — | | 0 | | — | — | 0 |
| 8 | — | 0 | — | 0 | — | 0 | — | — | 0 |

**Table 5 Natural frequencies for single- and two-ply rings**

| Mode no. | Natural frequency of cylindrical shells, Hz | | | | | | | |
|---|---|---|---|---|---|---|---|---|
| | Single-ply of PZT-4 | | | | Two-ply of Ti/PZT-4 | | | |
| | Open | $G$ | Closed | $G$ | Open | $G$ | Closed | $G$ |
| 1 | 22.1824 | 7 | 22.1489 | 7 | 32.1603 | 7 | 31.2691 | 7 |
| 2 | 22.1825 | 5 | 22.1490 | 5 | 32.1604 | 5 | 31.2691 | 5 |
| 3 | 35.7419 | 3 | 35.7311 | 3 | 54.0010 | 3 | 53.7213 | 3 |
| 4 | 35.7419 | 1 | 35.7311 | 1 | 54.0010 | 1 | 53.7213 | 1 |
| 5 | 62.8285 | 6 | 62.7342 | 6 | 91.1278 | 6 | 88.6404 | 6 |
| 6 | 90.5092 | 2 | 90.4655 | 2 | 135.7631 | 2 | 134.5059 | 2 |
| 7 | 120.6911 | 7 | 120.5112 | 7 | 175.1058 | 7 | 170.4211 | 5 |
| 8 | 120.6922 | 5 | 120.5118 | 5 | 175.1069 | 5 | 170.4211 | 7 |
| 9 | 155.9766 | 3 | 155.8808 | 3 | 232.5630 | 3 | 229.6163 | 1 |
| 10 | 155.9772 | 1 | 155.8811 | 1 | 232.5634 | 1 | 229.6163 | 3 |
| 11 | 195.6277 | 6 | 195.3356 | 6 | 283.9423 | 6 | 276.5251 | 6 |
| 12 | 234.8419 | 2 | 234.6776 | 2 | 348.5688 | 2 | 343.2685 | 2 |
| 13 | 287.7524 | 7 | 287.3244 | 7 | 417.9280 | 7 | 407.2865 | 7 |
| 14 | 287.7577 | 5 | 287.3274 | 5 | 417.9336 | 5 | 407.2866 | 5 |
| 15 | 329.1083 | 3 | 328.8641 | 3 | 486.9268 | 3 | 478.6454 | 1 |
| 16 | 329.1123 | 1 | 328.8661 | 1 | 486.9298 | 1 | 478.6455 | 3 |
| 17 | 397.3542 | 6 | 396.7744 | 6 | 577.6555 | 6 | 563.2648 | 6 |
| 18 | 439.9590 | 2 | 439.6247 | 2 | 649.5192 | 2 | 637.6491 | 2 |
| 19 | 524.8984 | 7 | 524.1785 | 7 | 763.9443 | 7 | 745.2069 | 7 |
| 20 | 524.9137 | 5 | 524.1871 | 5 | 763.9600 | 5 | 745.2070 | 5 |
| 21 | 568.1989 | 3 | 567.7761 | 3 | 837.6523 | 3 | 821.6142 | 3 |
| 22 | 568.2122 | 1 | 567.7836 | 1 | 837.6625 | 1 | 821.6142 | 1 |
| 23 | 671.0491 | 6 | 670.2028 | 6 | 977.7711 | 6 | 953.9783 | 6 |
| 24 | 714.5310 | 2 | 714.0170 | 2 | 1052.4301 | 2 | 1031.6462 | 2 |
| 25 | 836.4277 | 7 | 835.4825 | 7 | 1220.0096 | 7 | 1190.4773 | 5 |
| 26 | 836.4622 | 5 | 835.5026 | 5 | 1220.0432 | 5 | 1190.4779 | 7 |
| 27 | 863.0281 | 6 | 848.9344 | 6 | 1294.8354 | 3 | 1268.7792 | 1 |
| 28 | 879.5614 | 3 | 878.9708 | 3 | 1294.8599 | 1 | 1268.7795 | 3 |
| 29 | 879.5953 | 1 | 878.9918 | 1 | 1320.2649 | 6 | 1288.4930 | 6 |
| 30 | 1063.9916 | 2 | 1063.3160 | 2 | 1363.8622 | 7 | 1330.2111 | 7 |

for the modeled domain to completely determine the response spectra. This has been discussed in detail by Ohno.[37] These are defined here as groups 1–8, with the boundary conditions corresponding to each case listed in Table 4, with the symmetry planes along $x = 0$, $y = 0$, and $z = 0$ and the corresponding appropriate boundary conditions imposed along these surfaces.

Both open- and closed-circuit conditions are considered. The first 30 frequencies are shown in Table 5 along with the group, denoted as $G$, corresponding to the boundary conditions used. A number of these are repeated roots, which is consistent with the material symmetry used for the two cases. As is the case for similar comparisons, the open-circuit conditions yield a slightly higher frequency than do the corresponding closed-circuit conditions. The two-ply shell gives larger frequencies, primarily because of the larger stiffnesses of the passive material.

## Conclusions

A shell element for laminated piezoelectric shells has been constructed using a discrete-layer theory that allows discontinuous shear strains through the shell thickness and significant freedom in representing the through-thickness elastic and electric fields. The formulation is constructed in curvilinear coordinates and can be specialized to plates, cylindrical shells, or shells with arbitrary configuration. The accuracy of the element and formulation was established using comparisons with exact solutions for simply supported plates, with both static and free vibration characteristics being explored. The active and sensory response of a cylindrical ring also was studied.

Excellent agreement with exact solutions was obtained for the case of the plate with four discrete layers through the thickness providing sufficient accuracy. In static response for the cylindrical ring, the relationship between the induced displacements and applied voltage pattern was demonstrated for the cylindrical ring. In free vibration characteristics, the open-circuit frequencies were always slightly higher than the closed-condition values. Using the formulation presented here, more complicated loadings and geometries can be investigated, as can modified displacement and potential field approximations through the thickness.

## Acknowledgments

This work was supported by NASA Lewis Research Center under Grant NAG3-1520 and Cooperative Agreement NCC3-455. Dale A. Hopkins was the project monitor. The support is gratefully acknowledged.

## References

[1]Cady, W. G., *Piezoelectricity*, rev. ed., Vols. 1–2, Dover, New York, 1964.

[2]Nye, N. Y., *Physical Properties of Crystal: Their Representation by Tensors and Matrices*, Oxford Univ. Press, Oxford, England, UK, 1972.

[3]Tiersten, H. F., *Linear Piezoelectric Plate Vibrations*, Plenum, New York, 1969.

[4]Parton, V. Z., and Kudryavtsev, B. A., *Electromagnetoelasticity*, translated from Russian by E. G. Strel'chenko, Gordon and Breach, New York, 1988.

[5]Eer Nisse, E. P., "Resonances of One-Dimensional Composite Piezoelectric and Elastic Structures," *IEEE Transactions on Sonics and Ultrasonics*, Vol. SU-14, No. 2, 1967, pp. 59–67.

[6]Eer Nisse, E. P., "Variational Method for Electroelastic Vibration Analysis," *IEEE Transactions on Sonics and Ultrasonics*, Vol. SU-14, No. 5, 1967, pp. 153–160.

[7]Holland, R., "Resonant Properties of Piezoelectric Ceramic Rectangular Parallelepipeds," *Journal of the Acoustical Society of America*, Vol. 43, No. 5, 1968, pp. 988–997.

[8]Allik, H., and Hughes, T. J. R., "Finite Element Method for Piezoelectric Vibration," *International Journal for Numerical Methods in Engineering*, Vol. 2, 1970, pp. 151–157.

[9]Kagawa, Y., and Yamabuchi, T., "Finite Element Approach for a Piezoelectric Circular Rod," *IEEE Transactions on Sonics and Ultrasonics*, Vol. SU-23, No. 6, 1976, pp. 379–385.

[10]Naillon, M., Coursant, R. H., and Besnier, F., "Analysis of Piezoelectric Structures by a Finite Element Method," *Acta Electronica*, Vol. 25, 1983, pp. 341–362.

[11]Ostergaard, D. F., and Pawlak, T. P., "Three-Dimensional Finite Elements for Analyzing Piezoelectric Structures," *Proceedings of 1986 IEEE Ultrasonics Symposium*, Inst. of Electrical and Electronics Engineers, New York, 1986, pp. 639–644.

[12]Kunkel, H. A., Locke, S., and Pikeroen, B., "Finite-Element Analysis of Vibrational Modes in Piezoelectric Ceramic Disks," *IEEE Transactions on Ultrasonics, Ferroelectrics, and Frequency Control*, Vol. 37, No. 4, 1990, pp. 316–328.

[13]Tzou, H. S., and Gadre, M., "Theoretical Analysis of a Multi-Layered Thin Shell Coupled with Piezoelectric Shell Actuators for Distributed Vibration Controls," *Journal of Sound and Vibration*, Vol. 132, No. 3, 1989, pp. 433–450.

[14]Tzou, H. S., "Distributed Sensing and Controls of Flexible Plates and Shells Using Distributed Piezoelectric Elements," *Journal of Wave-Material Interaction*, Vol. 4, Nos. 1–3, 1989, pp. 11–29.

[15]Tzou, H. S., and Tseng, C. I., "Distributed Piezoelectric Sensor/Actuator Design for Dynamic Measurement/Control of Distributed Parameter Systems: A Piezoelectric Finite Element Approach," *Journal of Sound and Vibration*, Vol. 138, 1990, pp. 17–34.

[16]Tzou, H. S., and Zhong, J. P., "Adaptive Piezoelectric Shell Structures: Theory and Experiments," *Proceedings of the AIAA/ASME/ASCE/AHS/ASC 32nd Structures, Structural Dynamics, and Materials Conference* (Baltimore, MD), AIAA, Washington, DC, 1991, pp. 2290–2296 (AIAA Paper 91-1238).

[17]Tzou, H. S., *Piezoelectric Shells: Distributed Sensing and Control of Continua*, Kluwer Academic, Norwell, MA, 1993.

[18]Lammering, R., "Application of a Finite Shell Element for Composites Containing Piezo-electric Polymers in Vibration Control," *Computers and Structures*, Vol. 41, No. 5, 1991, pp. 1101–1109.

[19]Dökmeci, M. C., "Theory of Vibrations of Coated, Thermopiezoelectric Laminae," *Journal of Mathematical Physics*, Vol. 19, Jan. 1978, pp. 109–126.

[20]Dökmeci, M. C., "Shell Theory for Vibrations of Piezoceramics Under a Bias," *IEEE Transactions on Ultrasonics, Ferroelectrics, and Frequency Control*, Vol. 37, No. 5, 1990, pp. 369–385.

[21]Pagano, N. J., "Exact Solutions for Rectangular Bidirectional Composites and Sandwich Plates," *Journal of Composite Materials*, Vol. 4, Jan. 1970, pp. 20–34.

[22]Robbins, D. H., and Reddy, J. N., "Analysis of Piezoelectrically Actuated Beams Using a Layer-Wise Displacement Theory," *Computers and Structures*, Vol. 41, No. 2, 1991, pp. 265–279.

[23]Pauley, K. E., "Analysis of Plane Waves in Infinite Laminated, Piezoelectric Plates," Ph.D. Dissertation, Engineering, Univ. of California, Los Angeles, CA, 1974.

[24]Reddy, J. N., "A Generalization of Two-Dimensional Theories of Laminated Composite Plates," *Communication in Applied Numerical Methods*, Vol. 3, No. 2, 1987, pp. 113–180.

[25]Robbins, D. H., and Reddy, J. N., "Modelling of Thick Composites Using a Layerwise Laminate Theory," *International Journal for Numerical Methods in Engineering*, Vol. 36, No. 4, 1993, pp. 655–677.

[26]Heyliger, P. R., and Saravanos, D. A., "On Discrete-Layer Mechanics for Health Monitoring Application in Smart Composite Structures," *Adaptive Structures and Material Systems*, edited by G. P. Carman and E. Garcia, AD-Vol. 35, American Society of Mechanical Engineers, New York, 1993, pp. 303–312.

[27]Saravanos, D. A., Heyliger, P. R., and Hopkins, D. A., "Mechanics for the Coupled Dynamic Response of Active/Sensory Composite Structures," *Proceedings of the AIAA/ASME 35th Adaptive Structures Forum* (Hilton Head, SC), AIAA, Washington, DC, 1994 (AIAA Paper 94-1756).

[28]Heyliger, P. R., Ramirez, G., and Saravanos, D. A., "Coupled Discrete-Layer Finite Elements for Laminated Piezoelectric Plates," *Communications in Numerical Methods in Engineering*, Vol. 10, No. 12, 1994, pp. 971–981.

[29]Saravanos, D. A., and Heyliger, P. R., "Layerwise Analysis of Composite Beams with Embedded Piezoelectric Sensors and Actuators," *Journal of Intelligent Material Systems and Structures*, Vol. 6, No. 3, 1995, pp. 350–363.

[30]Hildebrand, F. B., *Advanced Calculus for Applications*, 2nd ed., Prentice–Hall, Englewood Cliffs, NJ, 1976, p. 308.

[31]Heyliger, P. R., Ramirez, G., and Pei, K. C., "Discrete-Layer Piezoelectric Plate and Shell Models for Active Tip Clearance Control," NASA CR 195383, 1994.

[32]Zienkiewicz, O. C., and Taylor, R. L., *The Finite Element Method*, Vol. 1, McGraw–Hill, London, 1988.

[33]Heyliger, P., "Static Behavior of Laminated Elastic/Piezoelectric Plates," *AIAA Journal*, Vol. 32, No. 12, 1994, pp. 2481–2484.

[34]Berlincourt, D. A., Curran, D. R., and Jaffe, H., "Piezoelectric and Piezomagnetic Materials and Their Function in Transducers," *Physical Acoustics: Principles and Methods*, Academic, New York, 1964.

[35]Tashiro, K., Tadokoro, H., and Kobayashi, M., "Structure and Piezoelectricity of Poly (Vinylidene Flouride)," *Ferroelectrics*, Vol. 32, Nos. 1–4, 1981, pp. 167–175.

[36]Heyliger, P. R., and Saravanos, D. A., "Exact Free Vibration Analysis of Laminated Plates with Embedded Piezoelectric Layers," *Journal of the Acoustical Society of America*, Vol. 98, No. 3, 1995, pp. 1547–1557.

[37]Ohno, I., "Free Vibration of a Rectangular Parallelepiped Crystal and Its Application to Determination of Elastic Constants of Orthorhombic Crystals," *Journal of the Physics of the Earth*, Vol. 24, 1976, pp. 355–379.